Structure and diffusion of intrinsic defect complexes in $LiNbO_3$ from density functional theory calculations

2010 J. Phys.: Condens. Matter 22 135002

(http://iopscience.iop.org/0953-8984/22/13/135002)

J. Phys.: Condens. Matter **22** (2010) 135002 (7pp) doi:10.1088/0953-8984/22/13/135002

Structure and diffusion of intrinsic defect complexes in $LiNbO_3$ from density functional theory calculations

Haixuan Xu[1], Donghwa Lee[1], Susan B Sinnott[1], Volkmar Dierolf[2], Venkatraman Gopalan[3] and Simon R Phillpot[1,4]

[1] Department of Materials Science and Engineering, University of Florida, Gainesville, FL 32611, USA
[2] Department of Physics, Lehigh University, Bethlehem, PA 18015, USA
[3] Department of Materials Science and Engineering, Pennsylvania State University, University Park, PA 16802, USA

E-mail: sphil@mse.ufl.edu

Received 6 January 2010, in final form 20 January 2010
Published 25 February 2010
Online at stacks.iop.org/JPhysCM/22/135002

Abstract
Organized defect clusters in non-stoichiometric $LiNbO_3$ are known to dominate macroscale ferroelectric properties; yet the detailed nature of these defects is currently unknown. Here, the relative stabilities of various defect cluster arrangements of lithium vacancies around a niobium antisite in $LiNbO_3$ are determined using density functional theory combined with thermodynamic calculations. Their effects on the ferroelectricity of the system are also discussed. It is found that at room temperature the non-uniaxial dipole moments associated with the defect clusters could affect the properties of the system locally. The diffusion mechanism is predicted to be through first nearest neighbor jumps on the Li sublattice. The diffusivity of the lithium vacancy is found to be extremely low at room temperature, which indicates that the defect complexes should be rather stable.

(Some figures in this article are in colour only in the electronic version)

1. Introduction

$LiNbO_3$ is one of the most technologically important oxides, with an extraordinary combination of ferroelectric, piezoelectric, acoustic, and optical properties [1, 2]. Much work has focused on the congruent composition of $LiNbO_3$ [3–5]. Recently, however, stoichiometric $LiNbO_3$ has been synthesized using the double crucible Czochralski (DCCZ) [6, 7] and vapor transport equilibration (VTE) methods [8–10]. The change of composition from the congruent (lithium poor) composition to the stoichiometric composition results in significant changes in the physical properties of the system, including the Curie temperature [11], the ferroelectric coercive field [11, 12], and the photorefractive properties [2]. These changes in physical properties are thought to be due to the point defects and defect clusters. Yet, very little is known about the detailed structure and energetics of such clusters.

There are three models for intrinsic point defect structures in $LiNbO_3$. In the first model (model I), two lithium vacancies are compensated by an oxygen vacancy ($2V'_{Li} + V^{\cdot\cdot}_{O}$) [13]. In the model II, niobium antisites are compensated by niobium vacancies ($5Nb^{\cdot\cdot\cdot\cdot}_{Li} + 4V^{''''}_{Nb}$) [14]. Model III, consists of a niobium antisite compensated by lithium vacancies, ($Nb^{\cdot\cdot\cdot\cdot}_{Li} + 4V'_{Li}$); this has been found to be dominant from experimental X-ray and neutron diffraction studies [6, 15–17] and density functional theory calculations [18]. Furthermore, Kim *et al* [19] proposed a plausible structure for model III in which the niobium antisite is surrounded by three lithium vacancies in nearest neighbor positions, plus one independent lithium vacancy along the z direction. Such defect clusters can possess a dipole moment that can lead to a local change in the polarization relative to that of the bulk system [20, 21]. Depending on whether the defect dipole is parallel or antiparallel to the ferroelectric polarization, the system may be in either an equilibrated or frustrated

[4] Author to whom any correspondence should be addressed.

state [2]. However, structural analysis suggests that many other arrangements of the Li vacancies are possible. In some arrangements, the polarization could also be more complicated than Kim's model, since it could have contributions in the plane normal to the uniaxial bulk polarization. A fundamental understanding of these local arrangements and the effects of these arrangements on the ferroelectricity is still lacking.

Here, density functional theory is combined with thermodynamic calculations to determine the relative stability of various defect cluster arrangements of lithium vacancies around a niobium antisite (model III). The various arrangements are classified based on how many lithium vacancies are in the first nearest neighbor position and on their positions relative to each other. In a previous DFT study it was found that a niobium antisite compensated by four lithium vacancies ($Nb_{Li}^{\cdots\cdot} + 4V'_{Li}$) is the dominant defect under Nb_2O_5-rich (i.e., congruent) conditions [18]; all calculations in this paper are thus performed under these conditions. The relative energies of a number of these configurations are calculated; because all of the configurations of this cluster have the same composition, these relative energies are independent of the thermodynamic reference state chosen. In order to predict whether such defect clusters are mobile or static, the energy barrier for migration and consequent diffusivity of lithium are obtained. Finally, the effects of the defect arrangement on the local net polarization are determined.

2. Methods

The first principles calculations are carried out using the projected augmented wave (PAW) method [22] combined with generalized gradient approximation (GGA), as implemented in the Vienna *ab initio* simulation package (VASP) [23, 24]. The Li $2s^1$, Nb $4p^6 4d^4 5s^1$, and O $2s^2 2p^4$ are treated as valence electrons. A $4 \times 4 \times 2$ Monkhorst–Pack [25] k-point mesh is used and the cut-off energy for the plane wave basis set is 400 eV [18]. The structure is optimized until the energies and forces are converged to 0.01 eV and 0.01 eV $Å^{-1}$. The computational supercell for all the calculations contains $2 \times 2 \times 2$ conventional unit cells, which amounts to 240 atoms with 1440 electrons.

The defect formation energy (DFE) of a defect or defects, α, with charge state q is defined as [26]

$$\Delta E_f(\alpha, q, T, P) = E^{\text{total}}(\alpha, q) - E^{\text{total}}(\text{perfect}) + \sum_i n_i \mu_i - q(\varepsilon_F + E_v + \Delta V), \quad (1)$$

where $E^{\text{total}}(\alpha, q, T, P)$ is the defect formation energy of defect α with charge state q; $E^{\text{total}}(\alpha, q)$ is the total energy obtained from DFT calculation of a supercell with the defect(s); $E^{\text{total}}(\text{perfect})$ is the total energy of the supercell without any defects. n_i is the number of atoms of species i that have been added to ($n_i > 0$) or removed from ($n_i < 0$) the supercell when the defects are created; μ_i is the chemical potential of element i. ε_F is the Fermi energy with respect to the valence band maximum in the bulk single crystal. E_v is the valence band maximum of the bulk single crystal. As discussed by Van de Walle and Neugebauer [26], a correction term ΔV, which is the difference in the electrostatic potentials of the defected and undefected systems, is needed to align the valence band maxima in the perfect and defected structures.

The dipole moment of the system is calculated using the conventional definition, which is the product of the magnitude of the charge with the distance between negative and positive charge [27]. To find the exact saddle point and the minimum energy path (MEP) between various crystallographically distinct variants of the defect cluster, transition state searches are carried out using the climbing image nudged elastic band (NEB) method [28, 29] implemented in VASP. The energy barrier is then calculated by taking the difference between the highest energy of the transition state and initial structure. For each possible diffusion path, eight images are employed, which is enough to obtain a good estimate of the MEP.

3. Structure and association effects

Both the niobium antisite and the lithium vacancies lie on the Li sublattice, therefore, the specific structure can be characterized in terms of this sublattice alone. The energetics is governed by the structural relaxation of all the ions in the cluster and the ions in its vicinity. Because there are so many possibilities, it is not feasible to characterize all the possible arrangements of the Li vacancies. However, the most important distinction is between arrangements in which the vacancies are very close to the Nb antisite and arrangements in which defects are a considerable distance apart. Thus, the clusters can be categorized in terms of the number of first nearest neighbors (FNNs), with the remaining vacancies further away.

(i) zero lithium vacancy as FNN and four far away (A0)
(ii) one lithium vacancy as FNN and three far away (A1)
(iii) two lithium vacancies as FNNs and two far away (A2)
(iv) three lithium vacancies as FNNs and one far way (A3)
(v) four lithium vacancies as FNNs (A4).

In the A0 structure, there is no association of the vacancies; this is the case analyzed previously and found to have negative formation energy for the Nb_2O_5 reference state [18]. For A1 and A2, only the lithium vacancies in the first nearest neighbor positions are explicitly included in the supercell calculation. For A3 and A4, to maintain the overall charge neutrality and characterize possible local charge effects, all the lithium vacancies are explicitly included in the supercell calculation. Taking A3 as an example, three lithium vacancies are in the FNN position while the fourth lithium vacancy is far away from defect cluster. The dependence of the DFE on the number of lithium vacancies in the FNNs of niobium antisite is given in figure 1. Because, as illustrated in the figure, the energy decreases with the number of FNNs, further analysis is focused on the A3 and A4 cases. Since there are six possible sites for the vacancies in the first neighbor shell, there are a number of structurally distinct variants of the A3 and A4 clusters. Each data point in figure 1 corresponds to a distinct configuration. The difference in energy between a given cluster and the A0 structure is the association energy of the cluster; Thus, the association energy for the various A4 cluster are all ~0.25 eV/defect. Because the association energies of the A3

Table 1. Defect formation energies and polarization of various A3 configurations. Kim-parallel represents that both defect and bulk have the same direction of polarization. Kim-antiparallel represents that the polarization direction of defect and bulk is opposite. The 1–2–3–8 and 4–5–6–7 configurations are illustrated in figures 2(a) and (b). All these models only possess polarization along [0001] direction. The bulk polarization is calculated to be 63.7 μC cm^{-2}, which is in excellent agreement with experimental value 62 $\pm$ 4 μC cm^{-2} base on near-stoichiometric sample [39]. The polarization of congruent $LiNbO_3$ is $\sim$71 μC cm^{-2} [40].

Defect cluster	DFE (eV/defect)	System polarization (μC cm^{-2})	Polarization change caused by defect clusters (μC cm^{-2})
4–5–6–8 (Kim-parallel) [19]	−1.222	60.5	−3.2
1–2–3–7 (Kim-antiparallel) [19]	−1.191	59.8	−3.9
1–2–3–8 (parallel)	−1.224	69.2	5.5
1–2–3–9 (parallel)	1.201	74.5	10.8
4–5–6–7 (antiparallel)	−1.223	60.6	−3.1

Table 2. Defect formation energies and polarization of various A4 configurations (see figure 2(c)). D^* represents degeneracy. Change in polarization represents that polarization changes caused by the defect cluster in [0001] direction using bulk as reference.

Defect cluster	Vacancy positions	D^*	DFE (eV/defect)	System polarization (μC cm^{-2})			Change in polarization (μC cm^{-2})
				$[2\bar{1}\bar{1}0]$	$[\bar{1}2\bar{1}0]$	[0001]	
A4–A	1–3–5–6	6	−1.296	3.5	3.4	61.6	−2.1
A4–B	1–2–3–5	3	−1.254	1.3	2.3	58.2	−5.5
A4–C	3–4–5–6	3	−1.294	0.3	0.0	61.6	−2.1
A4–D	1–2–5–6	3	−1.301	2.3	1.1	64.5	0.8

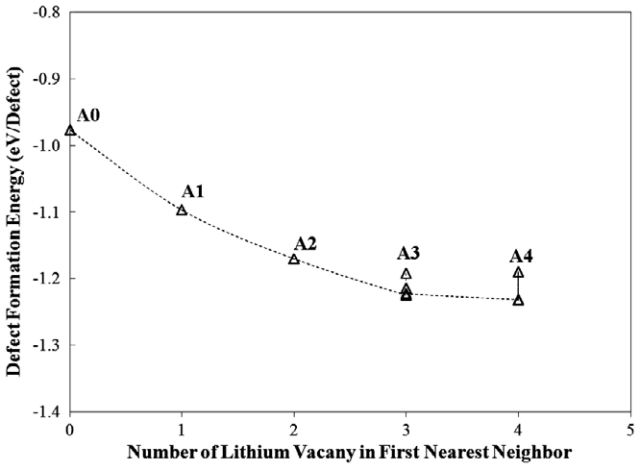

Figure 1. Defect formation energies dependence on the number of lithium vacancies in the first nearest neighbor positions of niobium antisite. For A3 and A4, the various points represent different configurations, as discussed in section 3.

and A4 structures are very similar, the energetics of a number of variants of each is examined in detail below.

Configuration A3. While there are a finite number of crystallographically distinct arrangements of the three FNN vacancies, the fourth 'far away' vacancy could be anywhere. One particular A3 model was proposed by Kim *et al* [19], in which the fourth Li vacancy lies along the z direction on the opposite side of the niobium antisite, as shown in figure 2(a). Two different configurations using Kim's model are considered in the present study: one in which the dipole moment of the cluster is parallel to the bulk ferroelectric polarization (4–5–6–8, Kim-parallel), the other with the defect dipole is antiparallel to the bulk polarization (1–2–3–7, Kim-antiparallel). The dipole moment of each system is shown in table 1, the Kim-parallel structure has a slightly lower energy (by 0.03 eV) than Kim-antiparallel structure. Because both of the structures preserve the rhombohedral symmetry of the system, there are no components of polarization orthogonal to the bulk uniaxial polarization; as a result, the polarization remains purely uniaxial.

In figure 2(b), three configurations have been proposed, which could yield much larger electric dipole moments of defect clusters than Kim's model (table 1). These correspond to vacancies on the 1–2–3–8, 1–2–3–9 and 4–5–6–7 sites, respectively. Cases 1–2–3–8 and 1–2–3–9 have dipole moments parallel to the bulk polarization direction while the dipole moment of 4–5–6–7 is antiparallel to the bulk polarization. These configurations are similar to Kim's model, in that three lithium vacancies lie in an FNN plane, (1, 2, and 3 in figure 2). However, they differ in the position of the fourth lithium vacancy (8 or 9), which in all cases lies on the same side of the Nb antisite as the plane of three Li FNN vacancies. The polarization and DFEs calculated based on these proposed configurations are given in table 1.

The comparison of the DFEs and polarizations of both Kim's model and the variants of the proposed configuration are also given in table 1. There is only $\sim$0.03 eV/defect difference between the highest and lowest energy variants. Table 1 does not show any clear relationship between the polarization and DFE. For the corresponding structures, such as parallel versus antiparallel Kim's model, the DFE decreases as the local polarization of the system (ferroelectric plus defect dipole) increases, which is consistent with the prediction of Gopalan *et al* [2]. However, it is not possible to compare structures because the difference in energy can be caused by both polarization and structural relaxations.

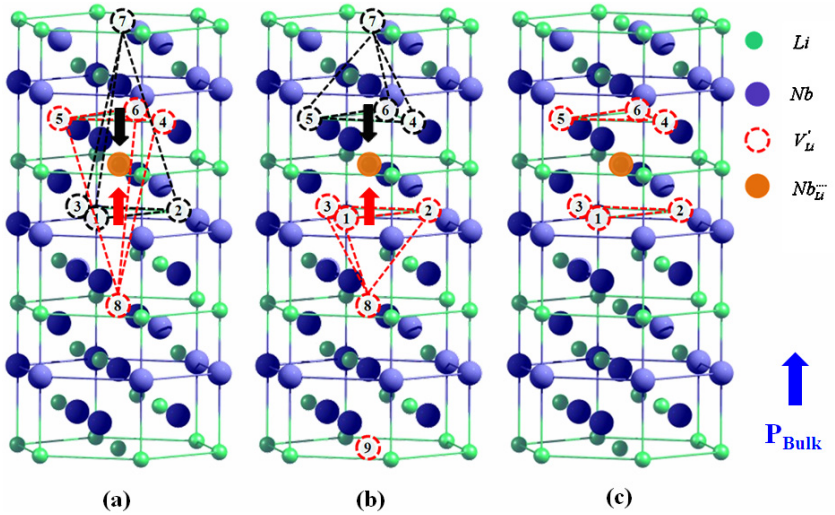

Figure 2. Local structure of niobium antisite. The bulk polarization direction is indicated at the right of the figure, shown in blue. The oxygen sublattice is not shown for clarity. (A) Kim's model: defect cluster 4–5–6–8 (red) is parallel to the bulk polarization direction; cluster 1–2–3–7 (black) is antiparallel to the bulk polarization direction. (B) Proposed configuration defect clusters 1–2–3–8 and 1–2–3–9 (red) are parallel to the bulk polarization direction with different value of dipole moment. Defect cluster 4–5–6–7 (black) is antiparallel to the bulk polarization direction. (C) Configurations of A4. 1–6 represent the six possible positions of lithium vacancies in the first near neighbors (FNNs). The dipole moment direction is from negative charged defect center (lithium vacancies) to positive charged defect center (niobium antisite).

Configuration A4. Taking four lithium atoms from six possible FNN positions yields fifteen ($C_6^4 = 15$) possible defect clusters. However, due to the three-fold symmetry of $LiNbO_3$ basal plane, only four of these configurations are distinct; these are listed in table 2 and illustrated in figure 2(c). All of these defect arrangements break the symmetry of the ferroelectric phase, thereby leading to non-uniaxial contributions to the polarization (see table 2). These non-uniaxial components are not negligible, amounting to up to 7.9% of the uniaxial component (for the A4–A structure). However, since all the symmetry equivalent structures of each of the four structures are equally likely, the system should maintain the overall, though not local, polarization of a bulk system as uniaxial, because the non-uniaxial contributions of an ensemble of defect clusters can be expected to cancel out.

As discussed in detail previously, the formation energy of defects depends on the physical conditions. In particular, experimentally, the properties of congruent (Li-poor) and stoichiometric $LiNbO_3$ are different from each other. In the thermodynamics calculations, the congruent case thus corresponds to using Nb_2O_5 as the reference state; correspondingly, the stoichiometric case corresponds to using Li_2O as the reference state. All of the above analysis has been for the Nb_2O_5 reference state. The DFE dependence on the reference state is given in figure 3. It can be seen that as reference state change from congruent (Nb_2O_5 such as Line EF in figure 3) to stoichiometric (Li_2O reference state, such as Line AD in figure 3) the DFEs change. As a result, the dominant defects change from niobium antisite compensated by lithium vacancies to lithium Frenkel pairs for the stoichiometric system. The positive value for DFE using the Nb_2O_5 reference may better represent the experimental condition of growth condition of congruent $LiNbO_3$.

The range of formation energies for these configurations is relatively small, only 0.05 eV/defect for A4. Thus, all such

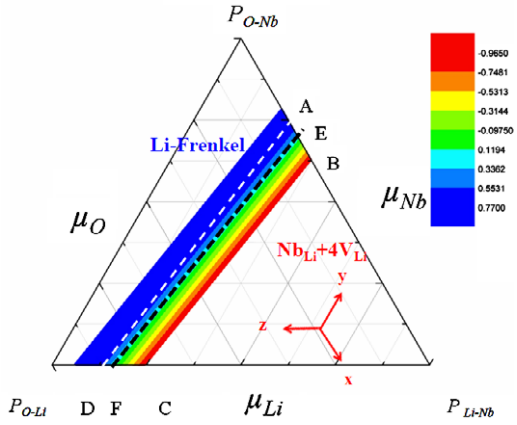

Figure 3. DFE dependence on chemical potential: the region in which Li Frenkel dominates is separated from the region where niobium antisite compensated by lithium vacancies dominates by the white-dot line. Line EF (black—dot) represents a condition that is considered to be close to the experimental growth condition of congruent lithium niobate.

configurations are likely to be present at room temperature. This can be seen explicitly by estimating the vibrational free energies of the various configurations. To calculate these, we have used lattice dynamics calculations at the level of the quasi-harmonic approximation, carried out using the using General Utility Lattice Program (GULP) [30, 31] with the empirical potential for $LiNbO_3$ by Araujo and Jackson [32]. The total difference in the vibrational free energy between perfect and the supercell crystal with the Nb antisite compensated by Li vacancies is calculated to be only 1.8% of the formation energy at room temperature; thermal effects therefore do not destabilize such a cluster. However, the range of vibrational free energies among the various configurations

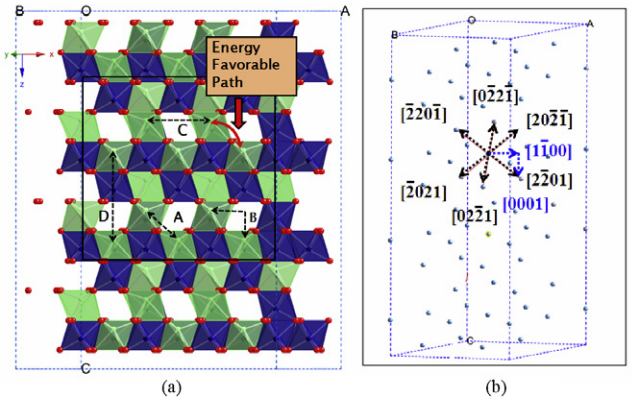

Figure 4. (a) Schematics of possible diffusion paths in the $LiNbO_3$, vertical direction is [000$\bar{1}$]. Diffusion path A represents the diffusion of lithium vacancy directly to its first nearest neighbor in the Li sublattice. Path B represents the diffusion through the vacant site then to its first nearest neighbor in the Li sublattice. Path C represents the diffusion within the basal plane. Path D is the diffusion of lithium vacancy directly along z direction, which is blocked by the niobium ions. The energy favorable path is highlighted with red and in solid line. (b) The diffusion direction of lithium vacancy to its six first nearest neighbor shown in three dimensions. This corresponds to the diffusion path A in the figure left (black).The diffusion path B is shown in blue. Only the Li sublattice is shown.

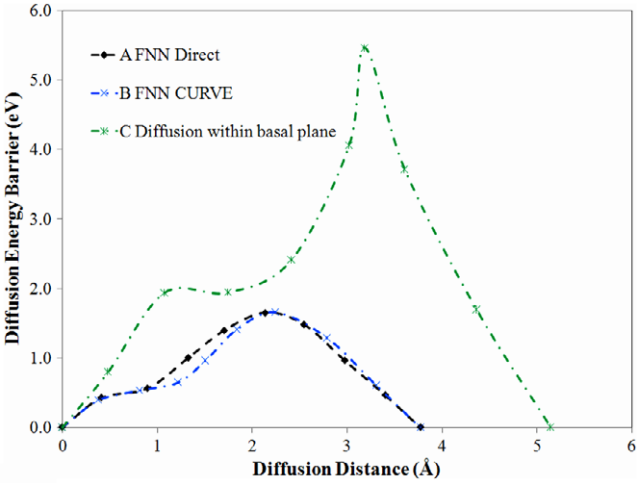

Figure 5. Nudged elastic band (NEB) calculations of diffusion barriers for lithium vacancy for several diffusion paths. Path A: *FNN direct* represents diffusion of lithium vacancy directly to its first nearest neighbor in the Li sublattice. Path B: *FNN curve* represents the diffusion through the vacant site then to its first nearest neighbor in the Li sublattice. Path C: represents the *diffusion within the basal plane*. Both path A and B converge to the energy favorable path indicated in figure 4 during the NEB calculation, in which the relaxation of the ions is considered.

is ∼0.1 eV at room temperature, confirming that each is likely to be present experimentally.

Because all the configurations can be expected to coexist in a real system, the polarization can be expected to include the effects of many defect configurations. Any comparison between simulation and experiments has to be treated with extreme caution because the dipole moments calculated in the present study represent an average over the simulation supercell. Thus, it represents a local polarization rather than the polarization averaged over a macroscopic region. It should also be noted that the dipole moments associated with the cluster will not switch orientation under domain reversal process unless there is a diffusive rearrangement of the ions in the cluster. The difficulty of rearranging the ions in the cluster could also cause domain-wall pinning by these defect clusters [33].

Diffusion of lithium vacancy and dynamics of defect complex

As the above analysis has shown, the DFEs of all of the A3 and A4 complexes are similar to each other. It is therefore of considerable interest to determine whether these structures can be expected to be long lived or whether the energy barriers to Li vacancy migration are sufficiently low that they might be highly dynamic, with Li vacancies diffusing among the various nearly energetically equivalent sites. If the defects are indeed dynamic, the non-uniaxial components of the polarization of each individual cluster may dynamically cancel out locally.

To set the context for this analysis, the diffusion of an isolated Li vacancy through the Li sublattice in $LiNbO_3$ is first considered. Based on a qualitative structural analysis, the energy barriers of several diffusion paths have been calculated (figure 4).

Path A. Diffusion of a lithium vacancy directly to its first Li nearest neighbor in the Li sublattice. Each Li ion has six first Li neighbors at a distance of 3.771 Å. Therefore, the jump direction for an individual Li ion can be any one of the following six directions: [02$\bar{2}$1], [$\bar{2}$021], [2$\bar{2}$01], [0$\bar{2}$2$\bar{1}$], [20$\bar{2}$$\bar{1}$], and [$\bar{2}20\bar{1}$]. As the diffusion directions maintain the three-fold symmetry, for both the plane above and below, the overall effect would lead to an isotropic diffusion mechanism.

Path B. Diffusion of a Li through the neighboring vacant site, then to its first nearest neighbor in the Li sublattice. For example, in figure 4(b), lithium vacancy first move towards [1$\bar{1}$00] then to [0 0 0 1] to reach [2$\bar{2}$01].

Path C. Diffusion within the basal plane. The diffusion distance for lithium vacancy within the basal plane (0001) is 5.138 Å along [$\bar{2}$110]. The coordination number of a vacancy is also six. However, this diffusion direction is perpendicular to the [0001] direction, which would lead to anisotropic diffusion mechanism.

The energy barriers associated with each of path A, B and C are given in figure 5. The energy barrier for diffusion within the basal plane (path C) is much higher than the values for diffusion between the first nearest neighbors of the Li sublattice (paths A and B). It is also observed that the diffusion path between the first nearest neighbors in the Li sublattice is neither straight (path A) nor exactly through the vacant site (path B), but is a compromise between the two. Furthermore, the diffusion barriers for this path is calculated to be 1.63 eV, which is in excellent agreement with the experimental values of the Li migration energy of 1.55 eV [34], 1.62 eV [35],

Table 3. Activation energy (E_a) obtained from first principles calculations, compared with the experimental results. The pre-factor (D_0) of the calculation is based on the assumption that the vibration frequency $\nu_0 \approx 2.5 \times 10^{13}$ s^{-1} and a jump distance between the first nearest neighbors of 3.771 Å. The diffusivity is calculated at $T = 1200$ K.

	Calculation	Experiment		
	(This work)	Mehta *et al* [34]	Halstead *et al* [35]	Schmidt *et al* [36]
D_0 (cm^2 s^{-1})	3.56×10^{-2}	5.10×10^{-1}	1.80×10^{-1}	2.10×10^{-2}
E_a (eV)	1.63	1.55	1.62	1.17
Diffusivity (cm^2 s^{-1})	5.10×10^{-9}	1.58×10^{-7}	2.84×10^{-8}	2.57×10^{-7}

and 1.17 eV [36] (table 3). This result is consistent with the conjecture that the diffusion mechanism in $LiNbO_3$ is through the migration of lithium vacancies on the Li sublattice [37].

The diffusivity of lithium vacancy can be calculated using the standard diffusion formula [27]

$$D_{\text{vac}} = \lambda^2 \nu_0 \exp\left(\frac{-\Delta H}{k_B T}\right) \tag{2}$$

where λ is the jump distance, ν_0 is the vibration frequency of the atoms, ΔH is the migration energy, k_B is the Boltzmann constant, and T is the temperature. Making the standard assumption [27], the vibration energy $h\nu_0$ is assumed to be the same as the thermal energy $k_B T$, where h is the Planck constant. The jump distance between the first nearest Li neighbors is 3.771 Å. At room temperature (298 K), the diffusivity is calculated to be 2.4×10^{-30} cm^2 s^{-1}, based on the DFT results. The diffusivity calculated from experimental data at room temperature is 3.2×10^{-27} cm^2 s^{-1} [34], 7.4×10^{-29} cm^2 s^{-1} [35], and 3.5×10^{-22} cm^2 s^{-1} [36] respectively. These are extremely low diffusion constants, which indicate that the defect clusters are rather stable at such temperature.

The average diffusion distance can then be calculated using the standard random walk equation:

$$x = \sqrt{6Dt} \tag{3}$$

where x is the diffusion distance, D is the diffusivity and t is the time. At room temperature, it requires years for lithium vacancy to diffuse in the order of angstroms. This indicates that each configuration of the defect complex should be very stable at room temperature, which may lead to significant local dipole moments, even including non-uniaxial contributions. However, after only five hours of annealing at 250 °C [38], the average diffusion distance is predicted to be in the order of tens of nanometers, which indicates the lithium vacancy should still be able to diffuse and sample different configurations of the defect complexes. This is consistent with the experimental observation that the relative peak emission intensities associated with defect structures measured by combined excitation emission spectroscopy can be modified by the annealing of the sample [38].

4. Conclusions

The stabilities of various energetically favored defect complex configurations have been investigated and a strong association between the niobium antisite and its compensating lithium vacancies has been observed. The dipole moment of each system has been calculated, with the dipole moments of the lowest energies clusters actually enhancing the local ferroelectric polarization, in contrast to the previous models that had predicted that clusters would decrease the polarization. This is consistent with the experimental observation that congruent $LiNbO_3$, in which niobium antisites and lithium vacancies should be abundant, has a higher polarization than that of stoichiometric $LiNbO_3$. Thus, the configurations proposed here could explain the discrepancy of polarization between the existing model and experimental data. Therefore, the net polarization of the system may be affected by all of the configurations. While over all this will result in an average uniaxial polarization, at room temperature the non-uniaxial dipole moments associated with the A4 clusters could affect the properties of the system locally and affect the domain-wall dynamics.

Several diffusion paths of lithium vacancies in $LiNbO_3$ were discussed. A diffusion mechanism through first nearest neighbor jumps on the Li sublattice was predicted to be the energetically favored path. The activation energy calculated based on this diffusion path is in excellent agreement with two of the three experimental values for lithium diffusion. The diffusivity of lithium vacancy was found to be extremely low at room temperature. However, the average diffusion distance was predicted to be on the order of tens of nanometers after five hour annealing at 250 °C, which indicates that lithium vacancies can still migrate through the system, thereby changing the local configurations of the defect complexes at elevated temperatures.

Acknowledgments

This work was supported by the National Science Foundation under Grant Numbers DMR-0602986 and DMR-0303279. We are happy to acknowledge computational resources provided by the high performance center (HPC) at the University of Florida.

References

[1] Wong K K 2002 *Properties of Lithium Niobate* (Stevenage: INSPEC)
[2] Gopalan V, Dierolf V and Scrymgeour D A 2007 *Annu. Rev. Mater. Res.* **37** 449
[3] Erdei S and Gabrieljan V T 1989 *Cryst. Res. Technol.* **24** 987
[4] Wang H L, Hang Y, Xu J, Zhang L H, Zhu S N and Zhu Y Y 2004 *Mater. Lett.* **58** 3119
[5] Abrahams S C and Marsh P 1986 *Acta Crystallogr.* B **42** 61

[6] Kitamura K, Yamamoto J K, Iyi N, Kimura S and Hayashi T 1992 *J. Cryst. Growth* **116** 327
[7] Kitamura K, Furukawa Y, Niwa K, Gopalan V and Mitchell T E 1998 *Appl. Phys. Lett.* **73** 3073
[8] Chen F S 1969 *J. Appl. Phys.* **40** 3389
[9] Holmes R J and Smyth D M 1984 *J. Appl. Phys.* **55** 3531
[10] Holman R L 1978 *Processing of Crystalline Ceramics* (New York: Plenum)
[11] Gopalan V and Gupta M C 1996 *Appl. Phys. Lett.* **68** 888
[12] Gopalan V, Mitchell T E, Furukawa Y and Kitamura K 1998 *Appl. Phys. Lett.* **72** 1981
[13] Prokhorov A and Kuzminov I 1990 *Physics and Chemistry of Crystalline Lithium Niobate* (Bristol: Hilger)
[14] Schirmer O F, Thiemann O and Wohlecke M 1991 *J. Phys. Chem. Solids* **52** 185
[15] Zotov N, Boysen H, Frey F, Metzger T and Born E 1994 *J. Phys. Chem. Solids* **55** 145
[16] Zhdanov G S, Ivanov S A, Kolontsova E V and Korneev A E 1978 *Ferroelectrics* **21** 463
[17] Ivanov S A, Korneyev A E, Kolontsova E V and Venevtsev Y N 1978 *Kristallografiya* **23** 1071
[18] Xu H X, Lee D, He J, Sinnott S B, Gopalan V, Dierolf V and Phillpot S R 2008 *Phys. Rev.* B **78** 174103
[19] Kim S, Gopalan V, Kitamura K and Furukawa Y 2001 *J. Appl. Phys.* **90** 2949
[20] Arlt G and Neumann H 1988 *Ferroelectrics* **87** 109
[21] Warren W L, Pike G E, Vanheusden K, Dimos D, Tuttle B A and Robertson J 1996 *J. Appl. Phys.* **79** 9250
[22] Blochl P E 1994 *Phys. Rev.* B **50** 17953
[23] Kresse G and Furthmuller J 1996 *Comput. Mater. Sci.* **6** 15
[24] Kresse G and Furthmuller J 1996 *Phys. Rev.* B **54** 11169
[25] Monkhorst H J and Pack J D 1976 *Phys. Rev.* B **13** 5188
[26] Van de Walle C G and Neugebauer J 2004 *J. Appl. Phys.* **95** 3851
[27] Barsoum M W 2002 *Fundamentals of Ceramics* (Bodmin: Taylor and Francis)
[28] Henkelman G, Uberuaga B P and Jonsson H 2000 *J. Chem. Phys.* **113** 9901
[29] Sheppard D, Terrell R and Henkelman G 2008 *J. Chem. Phys.* **128** 134106
[30] Gale J D 1997 *J. Chem. Soc. Faraday Trans.* **93** 629
[31] Gale J D and Rohl A L 2003 *Mol. Simul.* **29** 291
[32] Araujo R M, Lengyel K, Jackson R A, Kovacs L and Valerio M E G 2007 *J. Phys.: Condens. Matter* **19** 046211
[33] Meyer B and Vanderbilt D 2002 *Phys. Rev.* B **65** 104111
[34] Mehta A, Chang E K and Smyth D M 1991 *J. Mater. Res.* **6** 851
[35] Halstead T K 1970 *J. Chem. Phys.* **53** 3427
[36] Schmidt N, Betzler K, Grabs M, Kapphan S and Klose F 1989 *J. Appl. Phys.* **65** 1253
[37] Birnie D P 1993 *J. Mater. Sci.* **28** 302
[38] Dierolf V and Sandmann C 2007 *J. Lumin.* **125** 67
[39] Yao J H, Xu J J, Zhang G Y, Chen X J, Li B and Li G G 2000 *Chin. Phys. Lett.* **17** 513
[40] Byer R L 1997 *J. Nonlinear Opt. Phys. Mater.* **6** 549